REDUCTION OF THERMAL SHOCK INDUCED DAMAGES IN CARBON FIBER COMPOSITES

Jeremie Compan*, Takeshi Hirai*, Gerald Pintsuk*, Philipp Broxtermann, Nobuaki Noda***, Jochen Linke*, Lorenz Singheiser***

IEF2, Forschungszentrum Juelich, EURATOM Association, Germany

**** RWTH university, Aachen, Germany***

*****National Institute for Fusion Science, 322-6 Orosi-cho, Toki-shi 509-5292, Japan***

Keywords: *thermal damages, C/C composites, thermal shock, brittle destruction, ITER*

Abstract

Carbon Fiber Composites (CFCs) with graphitic matrix will act as a plasma facing material in the next step thermo-nuclear fusion device ITER. During plasma disruptions, they will be exposed to transient heat fluxes equivalent to a few GW.m^{-2} in a few ms. Simulation of these thermal loads was conducted on candidate materials in the electron-beam facility JUDITH. Influence of the fiber orientation (six different geometries were studied) on the thermal response and on the subsequent damages for the CFCs, have been investigated with respect to the material architecture. Less thermal shock induced damages, i.e. global (mostly atomic sublimation) and preferential erosion of the fibers perpendicular to the heat flux (governed by so-called brittle destruction processes), were observed in the newly proposed fiber orientations. Finite element modeling confirmed that already after a load duration of 1 ms, generated compressive stresses exceed the macroscopic material strength resulting in the material's brittle destruction.

1 General introdution

Carbon/carbon composites are foreseen to be used as plasma facing material (PFM) in the next step thermo-nuclear fusion device: ITER. These composites, so-called Carbon Fiber Composites (CFCs), have been developed to improve the thermal conductivity and the macroscopic mechanical strength of isotropic fine grain graphite (used for decades in fusion devices). CFCs have excellent thermo-mechanical properties in addition to inherent carbon properties, i.e. low atomic number and absence of melting. This makes CFCs very attractive PFMs for thermo-nuclear fusion devices [1]. The aim of PFMs in fusion confinement experiments is to remove the heat as fast as possible to the underlying cooling system in the plasma facing component (PFC) and this for the highest achievable number of cycles. In ITER, CFCs will be located in those regions where the highest heat fluxes are expected: the lower part of the divertor vertical targets. As part of the international negotiations between the seven partners for the construction of ITER, it has been decided that Japan will provide the CFC material for the vertical targets of the outer divertor and the European Union for the inner divertor (where deposited energies are lower, compared to the outer one, due to the ITER design [2]). Currently, on the European side, 7 CFC grades are in concurrency [3]. As the last phase of material qualification has arrived, no further grade will be developed and the selection has to be made among the available materials. Up to now, CFCs show the best performance of all potential PFMs in regard to their ability to sustain the expected loads in ITER during normal operations as well as during transient events [4]. However, under intense transient heat loads, CBMs will be damaged by the so-called brittle destruction (BD) process [5]. This phenomenon is caused by the anisotropy and the mismatch of coefficient of thermal expansion (CTE) between the different constituents of the CFCs i.e. matrix, fibers and fiber bundle layers. In addition to thermal erosion, BD leads to plasma contamination with a raising concern about tritium retention and early replacement of components. It has been demonstrated that fiber bundle layers oriented in the plane of the heat loaded surface are eroded and ejected preferentially under transient events [5]. Individual segmented carbon fibers or clusters of fibers are ejected during transient heat loads in the

GW.m^{-2} range for pulse durations of a few ms (characteristic for ITER-like disruptions) [4, 6]. One way to limit this type of damage is to decrease the amount of fibers aligned parallel to the loaded-surface plane by an appropriate cutting of the material i.e. an optimization of the fiber orientation. Due to the fact that inclined fibers can remove the heat deeper into the bulk, local overheating and thus further induced thermal stresses leading to BD can be avoided. First results demonstrated the benefit of this optimization route [7]. Further improvements in respect to materials architecture are presented here.

2 CFC materials

Two advanced CFCs have been used in this study: NB31 (SNECMA, France) and CX2002U (TOYO TANSO, Japan) (Fig. 1).

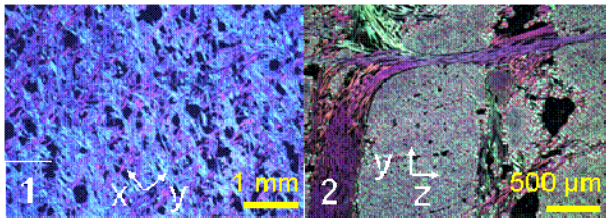

Fig. 1: Polarized light micrographs of 1) CX2002U and 2) NB31. These materials have orthotropic fiber orientations.

NB31 is an orthotropic 3-directional material composed of pitch fibers (27 vol. %, x-direction) providing a high thermal conductivity for the heat flux removal and PolyAcryloNitrile (PAN) fibers in y-direction (6 vol. %). This material is reinforced by needling of the PAN fibers in the z-direction (2 vol. %) (Fig. 2).

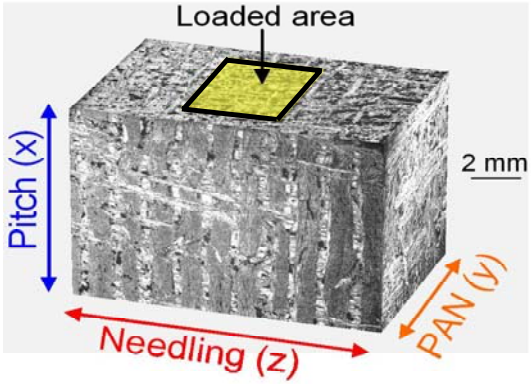

Fig. 2: Image showing the fiber orientations of NB31 loaded in the x-direction.

CX2002U is a 2-directional felt-type material composed of PAN fibers. These fibers are randomly disposed in two planes which are densified by chemical vapor deposition of pyrocarbon [8-9]. In contrast to NB31, no bundle (thousands of fibers packed as a unit; see Fig. 1)) structure is used in this material.

Typically, the materials are oriented in that way, that the direction of highest thermal conductivity (x) is parallel to the applied heat flux (Table 1, A). In addition to this standard orientation, thermal shock samples with fibers oriented at various angles were prepared in order to improve the heat removal efficiency, to tailor the mechanical properties, and therefore to reduce the preferential erosion in CFCs. Samples oriented at six different angles, as described in table 1, were manufactured from NB31 and CX2002U. An example for a tilted material is shown in Fig. 3 representing NB31 in the D orientation.

Table 1: Description of the used CFC orientations in respect to the three original orthotropic directions: x, y and z. The angle represents the orientation of the particular direction versus the direction of the incoming heat flux.

	A	B	C	D	E	F
x	0°	90°	90°	45°	30°	15°
y	90°	0°	90°	45°	60°	75°
z	90°	90°	0°	90°	90°	90°
	Basic orientations			Inclined fibers		

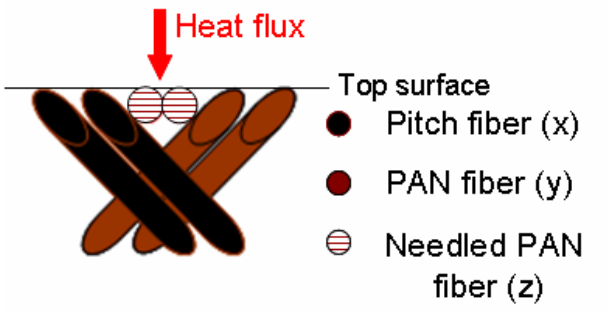

Fig. 3: Sketch of NB31 in the D orientation.

3 Experimental

In order to simulate the transient heat loads which are expected in large fusion devices, the electron beam test facility JUDITH (Juelich, Germany) was utilized. Thanks to a focused beam (of ~1 mm diameter) and a fast scanning mode of the surface (typically 40 to 60 kHz), homogeneous heating in a defined area (Fig. 2) is realized. JUDITH is able to simulate ITER-relevant disruptions loads.

In the experiments, each sample (12x12 mm^2, 5 mm thickness) was loaded at four different positions with identical loading conditions. This allows limiting the influence of the local microstructure of

the CFCs. Each loaded spot had a size of 4x4 mm^2. During and after the experiments, different diagnostics were used to monitor the applied parameters and the material response:
-The current absorbed by the sample was monitored in order to determine the absorbed power density.
-The surface temperature during the thermal shock load was measured by means of a single color fast pyrometer [6], providing a measurement spot of 3-4 mm in diameter, which was adjusted to the center of the loaded area.
-A CCD camera, dedicated to observe the emission of hot particles, was used to acquire time integrated pictures.
-Weight measurements were done before and after thermal shock loads following a baking of the samples for 3 hours in air to limit the influence of the water uptake.
-High resolution mechanical profilometry data were acquired with an Alpha-Step IQ facility from KLA Tencor. The height resolution was less than 1 µm.
- SEM analysis was performed after e-beam loading.

Extensive tensile [10] and 3-point bending tests of CFC materials were performed in different orientations in order to obtain the scattering of data and to be able to better characterize destruction processes under macroscopically controlled loads [11].

4 Results and discussion

4.1 Thermal shock tests

Transient thermal loads at power densities between 1.8 and 2.7 $GW.m^{-2}$ were applied for a pulse duration of 5 ms in order to simulate ITER-like disruptions. The experiments were single shot loads done at room temperature on non-cooled samples for the different orientations described in table 1.

Exemplarily, the time integrated CCD pictures of 3 out of 6 different orientations; i.e. the original, the worst and the best ones in terms of visible particle emission; of the CFC materials loaded at about 2.5 $GW.m^{-2}$ for 5 ms are presented in Fig. 4. The bright lines indicate the trajectories of hot particles, which have been released due to BD. For NB31, on the one hand, the amount of hot particles ejected from the sample significantly increased for the C in comparison to the A orientation, representing the standard orientation. This is related to the lower thermal conductivity in this direction [10], and also to the higher volumetric percentage of fibers aligned parallel to the loaded-surface plane compared to A. On the other hand, the CCD picture of an equivalent loading on E clearly demonstrates the emission of much less hot particles. In this respect, the E orientation has shown the best performance for NB31.

CX2002U was loaded at the same conditions and the results slightly differ from NB31. Due to its 2-D architecture and in contrast to NB31, A and B have almost the same thermo-mechanical properties [8-9] and therefore the thermal response is quasi-equivalent in these two directions (see Fig. 5). In the C orientation, the BD is higher as a consequence of the low thermal conductivity and mechanical properties in this direction [8-9]. Differently from NB31, for CX2002U the F orientation shows the lowest number of emitted particles.

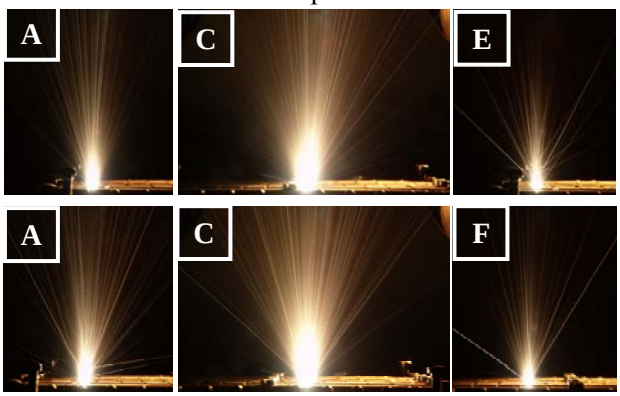

Fig. 4: Time integrated CCD pictures of NB31 (upper line) and CX2002U (lower line) during disruption loads of 2.5 $GW.m^{-2}$ for 5 ms. Orientations are indicated.

Fig. 5 displays the weight loss of NB31 and CX2002U in the particular directions A to F averaged for all applied thermal loads. This figure describes the same tendencies as described above and especially the anisotropic behavior of NB31 in the A, B and C orientations which leads to very diverse weight losses is clearly displayed.

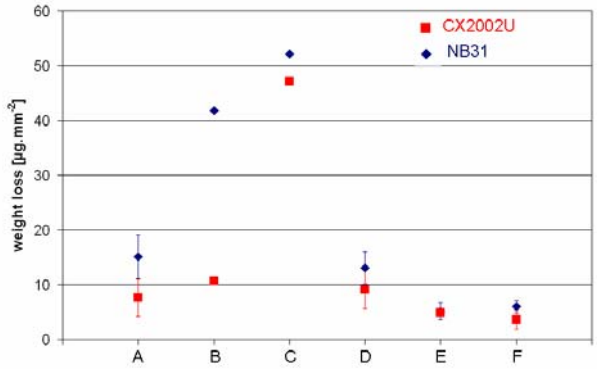

Fig. 5: Weight loss of NB31 and CX2002U in the respective orientation averaged for all applied loads from 1.8 to 2.7 $GW.m^{-2}$. The error bars represent the single averaged deviations.

The conclusion from these experimental results is that, in terms of weight loss CX2002U has for each tested direction a better thermal shock resistance than NB31. In addition, the scattering of values (related to the different absorbed power densities) is low for the orientations D to G but this will be the subject of a future study.

In SEM micrographs, taken from the loaded surface of the specimens (2.5 GW.m^{-2}, 5 ms) in the orientations D to F, only slight differences can be observed for NB31. The PAN fibers (y- and z-directions) were damaged preferentially, but via SEM a difference in the level of damage among these samples can hardly be determined. In contrast, for CX2002U, it was found that the orientation D exhibit apparently larger damages than E and F (cf. Fig. 6).

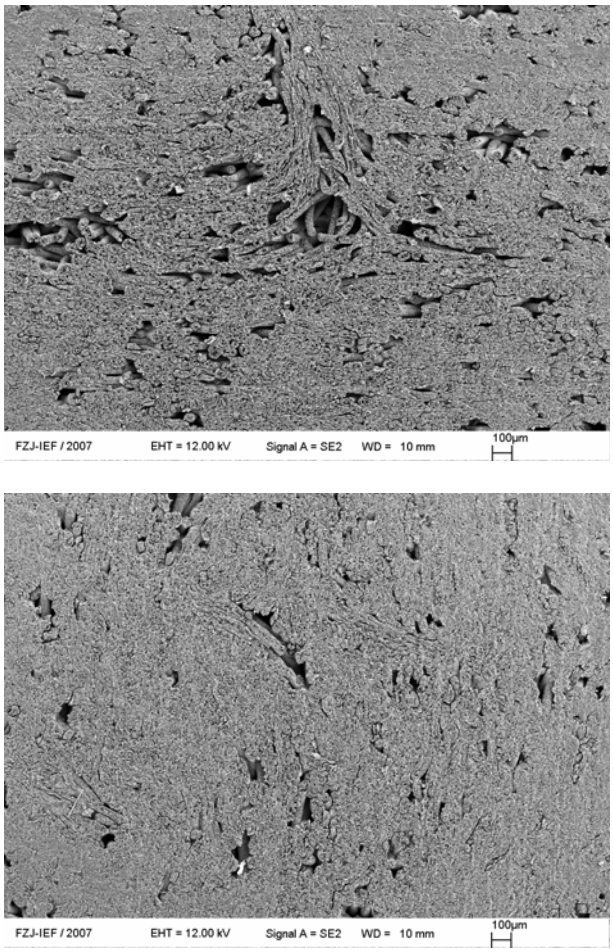

Fig. 6: Top view SEM micrographs of the loaded surface area of CX2002U after disruption loads of 2.5 GW.m^{-2} and 5 ms. Orientations D (top) and F (bottom) are displayed.

Three linear surface profiles of 10 mm in length (with a spatial resolution of 0.2 µm) were taken across two identically loaded positions of each sample. The spacing between the profiles was about 0.5 mm (examples of untreated profiles can be found in [7]). From these profiles reliable statistics on the erosion depth could be done by defining more than 100000 points acquired during all profilometry experiments as 100%. Within these 100%, all the points between -5 and +5 µm were not considered as they represent the original surface roughness and the uncertainty of the measurement. The results for NB31 are summarized in Fig. 7. Unfortunately, this way to process the data restricts the interpretation concerning the absolute number and the location (function of the CFC microstructure) of the formed craters as done in [7].

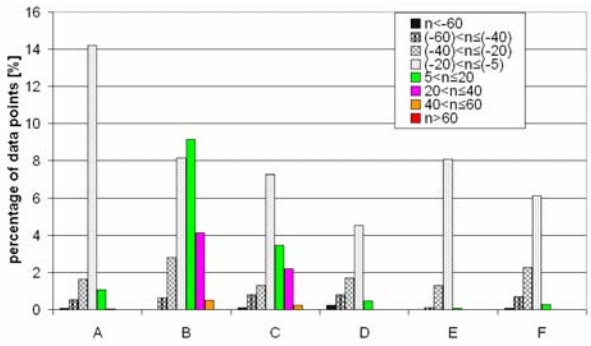

Fig. 7: NB31 (directions A to F); statistics on the number of points at a relative height 'n' (P = 2.5 GW.m^{-2}, t = 5 ms); range size: 20 µm

The A orientation shows mainly shallow erosion and few pulled-out fibers while for B quantitatively less data points corresponding to a shallow erosion (-5 to -20 µm) were found but significantly more pulled-out fibers. For C, the number of pulled-out fibers is lower than for B, but data points with values below -40 µm are increasing.

Observing the newly proposed orientations, i.e. D to F, they exhibit less heat-affected surfaces than the original orientation A. D orientation shows a good behavior similar to the one of the standard orientation although the fiber orientation would implicate that the result should be an intermediate behavior between A and B. This is a consequence of the four times higher content of pitch fibers than of PAN fibers, exhibiting an accordingly larger influence on the material behavior. The E orientation is obviously the orientation with almost no data below -40 µm and also above 5 µm. This is in correlation with all other experimental results. Reducing the deviation angle of the x-direction further to 15° as it was done for 'F', again an increase of data points < -40 µm is observed.

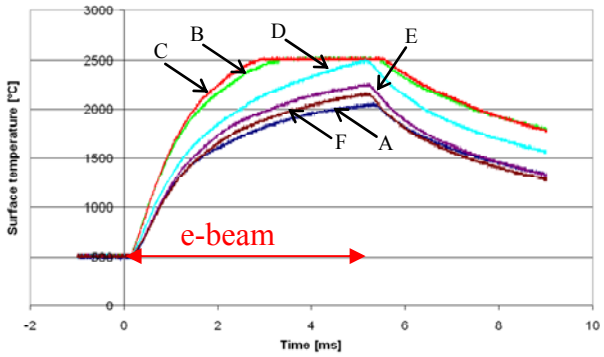

Fig. 8: Surface temperatures of NB31 during single shot 2.5 GW.m^{-2} for 5 ms in orientations A to G.

The surface temperatures of NB31 loaded with about 2.5 GW.m^{-2} for 5 ms are displayed in Fig. 8. Two parameters are important in such curves: the slope of the temperature during the heating phase as a function of time and the relative difference of the achieved maximum temperature between two orientations. It should be noticed that the emissivity of NB31 was set to $\varepsilon = 1$ and the temperature range of the pyrometer measurement was from 500 to 2500°C. A separation into two groups is determined whereby one consists of the orientations B and C showing a significantly faster temperature increase than the rest. For these two orientations the applied heat flux is parallel to the PAN-fiber directions (y or z) with low thermal conductivity; this explains a fast increase of the temperature and a very high maximum temperature even above the measurement range. Among the other orientations, the temperature is increasing according to the increase of the angle, indicating the deviation from the standard direction.

As a conclusion, the optimal orientation for NB31 among the proposed ones is E. For this orientation the mechanical attachment of the PAN fibers is, due the angle between the PAN fibers and the loaded surface, superior than in case of A resulting in a higher energy threshold for the ejection of particles; the number of released particles and the surface roughness are the lowest in this study for NB31.

For CX2002U, the optimal studied orientation in regard of the number of ejected particles, weight loss and surface roughening is F. This means that, compared to NB31, the orientation angle combining an optimal attachment of the fibers from the y direction and a high thermal conductivity of the loaded surface is closer to the standard orientation A. This can be linked to the felt type fiber preform used for the production of CX2002U where no fiber bundle is present, which should result in lower compressive stresses at the respective interfaces (see part 4.2). Nevertheless, as shown in Fig. 10, ejection of intersected single fibers also takes place.

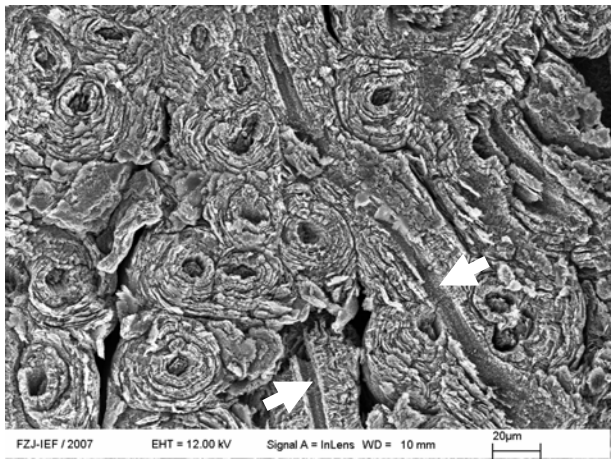

Fig. 9: Top view SEM micrograph of CX2002U (E orientation) after 2.5 GW.m^{-2} for 5 ms. The previous locations of two ejected fibers are indicated by arrows.

Generally, as described in [12], the inclination of the fibers can lead to hot spots in some corners of a PFM. Therefore the influence of the material's tilting in the xy-plane on the thermal performance under static loading especially at the material edges still has to be determined on actively cooled components.

4.2 Interpretation of enhanced brittle destruction in CFCs

It is well known that graphitic materials are highly anisotropic in terms of thermal and mechanical properties. In the graphene plane directions, thermal conductivity and mechanical strength are high whereas they are low in the transverse direction. In addition, the longitudinal CTE of highly oriented graphitic materials at room temperature is around -1x10^{-6} K^{-1} but transversally (to the graphene planes), it is around 26x10^{-6} K^{-1}. For carbon fibers in general, the graphene planes are aligned in the longitudinal direction and especially for both tested CFC-materials, the graphene planes of the matrix are concentrically surrounding the fibers. This multi-scale anisotropy causes stresses at the various interfaces during thermal loading. While fibers aligned in the loaded-surface plane overheat (location 1, Fig. 10) and expand, through the fibers oriented perpendicular to the surface (with higher thermal conductivity than the others; see [10]), the heat can propagate deeper into the bulk and thus they expand less (transversally) and even shrink (longitudinally). Since they will constrain the

expanded fibers (y- and z-directions) as shown in location 1, Fig. 10 consequently compressive stresses will be generated at the local interfaces. It is believed that the unbalanced volumetric percentage of fibers enhances these stresses. A way to release this compressive stresses is to generate longitudinal cracks (at the weakest positions) and pull-out these parts of fiber bundles after delamination [Fig. 11].

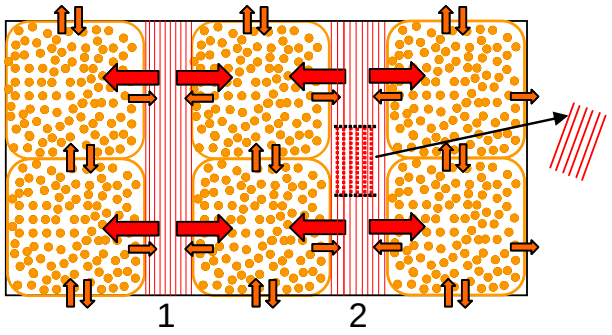

Fig. 10: Sketch of NB31 (needling direction (z) is not represented). Top view of the original direction (x) facing the heat flux during a heating-up phase. The red (hotter) lines are the PAN fibers and the orange (cooler) points are the cross-sections of the pitch fibers. The arrows represent the thermal expansion and their size their relative amplitudes.

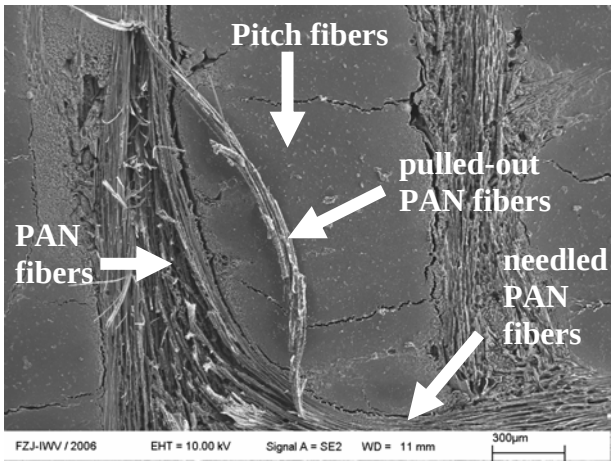

Fig. 11: Top view SEM micrograph of NB31 (A orientation) after about 2.7 GW.m^{-2} for 5 ms.

Due to the overheating of these fibers and after the loss of contact following delamination or a pulling-out, they shrink by generating transversal cracks allowing the ejection of these intersected fiber bundles (Fig. 10 part 2) [6]. To avoid this preferential erosion of fibers aligned in the loaded-surface plane all fibers have to be oriented in an optimized way, so that on the one hand the heat can diffuse along the fibers into the bulk and on the other a good mechanical attachment is achieved. Besides thermo-mechanical properties also the type of architecture of the used CFC is believed to strongly influence the enhanced BD. The fact that CX2002U is not constituted of large bundles of fibers like NB31, that its fiber content is quasi equivalent in x- and y-directions and that only one type of fiber is used will limit the stresses at the interface and will reduce the particle erosion, which is confirmed by the experimental results shown above.

4.3 Finite Element Modeling

The numerical simulation of thermal shock loading on the different materials was performed by Finite Element Modeling (FEM) using thermal and elastic-plastic analyses. Tensile properties have been acquired at room temperature [10] and were extrapolated for high temperatures following the tendency of graphitic materials to become stronger at higher temperatures [13]. The materials were assumed as homogeneous anisotropic materials.

In order to perform calculations, several parameters as a function of temperature are needed: CTE, thermal conductivity, Young's modulus (for the three orthotropic directions of CFCs) but also the heat capacity and the density. In addition, the Poisson's ratio ν and the shear modulus μ of the three directions had to be used. Unfortunately, such shear tests could not be done, thus in respect to [14] and the commonly used equation for a homogeneous isotropic material (Eq. 1), a shear modulus inferior to the Young's modulus E was suggested. Shear moduli equal to the Young's modulus, to the fifth and to the tenth of it were used in the code to monitor the influence of this value on the generated compressive stresses during the heating phase.

$$\mu = \frac{E}{(1+\nu)} \qquad (1)$$

As a first step of the analysis the measured surface temperature was fit to the measured temperature curves. As a matter of fact, if 2.7 GW.m^{-2} are input in the code the surface reaches temperatures higher than 7000K after 5 ms. It was calculated [15] that the surface of carbon based materials should reach temperatures of about 4000K under ITER-like disruptions. This means that, if we assume the calculations reasonable, the absolute surface temperatures are not correctly measured at high temperatures with our actual pyrometer. The reasons for this are still under investigation and will not be discussed here. Thus just the evolution of the slope of the measured surface temperature curves

can be correlated to the real material performance under disruption like loads (if assumed that the crater depth does not significantly influence the measurement). The decrease of the slope of the surface temperature (as a function of time) may indicate an increase of energy release from the loaded surface. This energy can be released not only by thermal radiation but also by atomic sublimation or ejection of hot particles due to BD. These two additional processes are not included in this calculation. Here should be pointed out that, regarding the vapour cloud shielding effect, it should be considered that the applied thermal load is done by electrons, with an energy of 120 keV, which will not be affected by the carbon vapour cloud above the surface. One conclusion from this is, that damages created by JUDITH will be larger than in a thermo-nuclear fusion device, where the incident power will be partially shielded by the vapour cloud. Thermal shock results obtained from JUDITH are thus considered as upper limits for material damages at these power densities.

Within the calculation, the 5 ms shot was subdivided in 6 parts in order to allow fitting due to the change of slope as a function of time. The input power densities were much lower (between 0.8 and 0.5 GW.m^{-2}) than the one measured (2.7 GW.m^{-2}) via the absorbed current through the sample.

Calculation performed for the A orientation of NB31 showed quasi constant stresses generated for the different selected values of shear moduli. A value fixed to the fifth of Young's modulus was found as a good compromise and applied for the two materials in each direction.

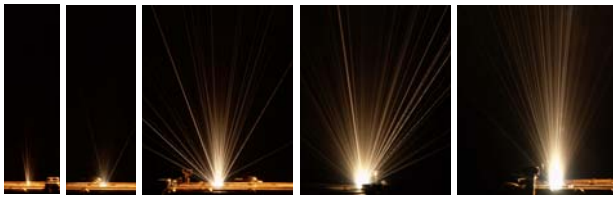

Fig. 12: NB31 in the A orientation; CCD time integrated images of the particle erosion during a load of 2.7GW.m^{-2} for 1 (left) to 5 ms (right).

In order to correlate the FEM calculations to the experimental results, 4 shots each of 1,2,3,4 and 5 ms with a power density of 2.7 GW.m^{-2} were additionally performed on NB31 (orientation A). In Fig. 12, one can see that hot particle release due to BD already slightly starts after 1 ms and increases drastically between the 2nd and the 3rd ms for 2.7 GW.m^{-2}. The weight loss measurements confirm (Fig. 13) and point out a significant weight loss increase between the 2nd and the 3rd ms, plus another weight loss augmentation between the 4th and the 5th ms.

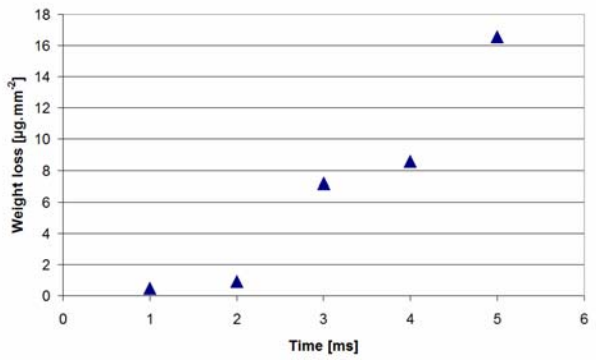

Fig. 13: Weight loss for NB31 under 2.7 GW.m^{-2} for different exposure times.

If we now correlate this with the surface temperatures (Fig. 14) then we observe a large change of slope between the 2nd and the 3rd ms indicating a change of regime for energy release from the loaded surface (by sublimation and/or BD).

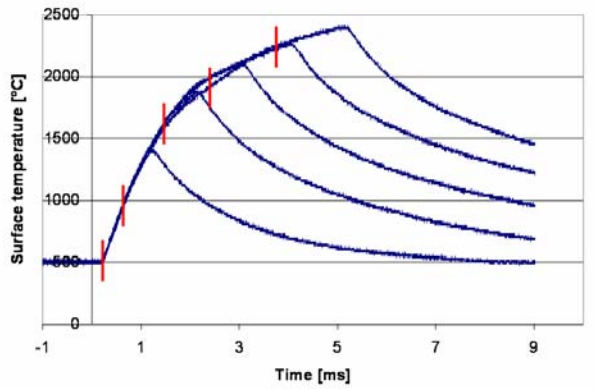

Fig. 13: Surface temperatures measured during independent loadings of 1,2,3,4 and 5 ms at 2.7GW.m^{-2}. The red lines represent the considered positions where the power density was fitted in the FEM calculations.

Induced thermal stresses were calculated for the different pulse durations for NB31 and 5 ms for CX2002U (orientation A). High compressive stresses are generated at the loaded area. The calculated stresses for each direction were normalized by the respective compressive strength of the materials [13] and plotted in Fig. 15. For NB31, it is clearly seen that stresses exceed the compressive strength of the material in y- and z-direction but never in the x-direction. One should also notice a clear increase of the stresses in between the 1st and the 2nd ms of loading. This is a bit earlier than observed in Fig. 11 but confirm a certain

boarder where the stresses drastically increase and then get constant until the 5th ms. This behaviour is linked to the very fast surface temperature increase during the two first ms (more than 1500° measured during loading). The second increase of weight loss which was shown in Fig. 13 between the 4th and the 5th can not be explained by these calculations. This evolution might be related to a scattering of the weight loss value (see Fig. 5).

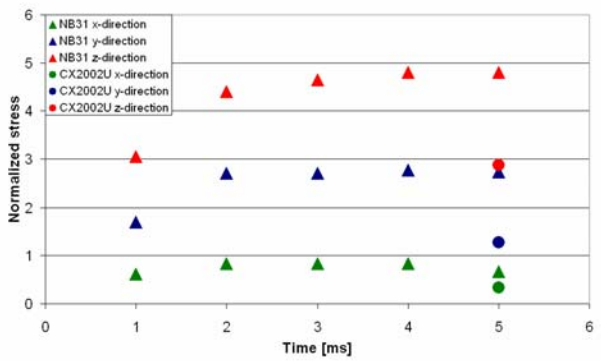

Fig. 15: Ratio of the calculated maximum compressive stress by the compressive strength as a function of time for NB31 and CX2002U in different directions.

For CX2002U after 5 ms, it was also observed that the thermal stresses exceed the material compressive strength in the y- and z- but not in x-direction. In addition, with respect to each direction, the normalized stresses are lower in the case of CX2002U. For both materials, the stresses generated in the z-direction are higher than in the y one. The z direction has the lowest mechanical properties and the lowest thermal conductivity leading to higher thermal gradients. This FEM estimation correlate the experimentally observed superiority of CX2002U over NB31 and the phenomena of BD (cracking of individual or bundles of fibers in y- and/or z-directions) observed for these materials under disruption loads.

Further improvement in the calculation can be done by quantifying and distinguishing the part of the energy release by sublimation and by BD with loading conditions where no particle emission is observed.

5 Conclusion

In this work, it was shown that the available CFCs for ITER can be improved in terms of weight loss under disruption loads by selecting the appropriate material orientation. The aim was to demonstrate that a better balance between the mechanical attachment of the fibers used to reinforce the structure (in y and z directions) and a sufficient thermal conductivity in the direction being parallel to the heat flux can limit brittle destruction (BD). In the case of NB31, the optimal direction was found to be the one tilted by 30° in the xy-plane in relation to the original orientation (x-direction parallel to the heat flux). The used preform for the production of CX2002U is different from the one of NB31 and the best studied orientation for CX2002U is a one closer to the original direction facing the heat flux, i.e. a rotation of 15° in the xy-plane. This shallower optimal angle is explained by a lower stress formation at the various interfaces due to the use of a felt type preform not a bundle type one like NB31, the quasi equivalent fiber content in x- and y-directions and the fact that only one type of fiber is used.

FEM analysis on NB31 in its original orientation (x) demonstrated that a sudden increase of compressive stresses occurs at the early stage of a disruption (where the temperature ramping is the highest) and stays stable after that. This is confirmed by the observation, that during a single shot of 2.5 $GW.m^{-2}$, BD starts as early as before the 1st ms and drastically increases between the 2nd and the 3rd ms. The thermal compressive stresses in the y- and z-directions always exceeded the material's strength meaning that fiber breakage can occur even within the first ms of the loading. The same calculations were done for CX2002U showing the superior thermo-mechanical behavior of CX2002U which confirms the experimental results. Since the energy release from the loaded surface by sublimation and BD were not implemented in the FEM-code, further improvements have to be done to optimize the use of this tool.

Acknowledgements

This work, supported by the European Communities under the contract of Association between EURATOM/FZJ, was carried out within the framework of the European Fusion Development Agreement. The views and opinions expressed herein do not necessarily reflect those of the European Commission.

References

[1] Tanabe T., "On the possibility of ITER starting with full carbon", *Fusion Engineering and Design*, 81, pp 139-147, 2006

[2] Petschanyi S. and Landman I., "ELM induced carbon contamination of ITER core", *J. Nucl. Mater.*, accepted proof, 2007

[3] Peacock A. T. et al., "Status of CFC development in Europe for ITER", *Physica Scripta*, T128, pp 23-28, 2007

[4] Hirai T. et al., "ITER relevant high heat flux testing on plasma facing surfaces", *Materials Transactions*, Vol. 46, No. 3, pp 412-424, 2005

[5] Hirai T. et al., "Particle release from carbon based materials under intense transient heat loads", *Physica Scripta*, Vol. T111, pp 163-166, 2004.

[6] Linke J. et al., "High heat flux simulation experiments with improved electron beam diagnostics". *J. Nucl. Mater.*, Vol. 283-287, pp 1152-1156, 2000.

[7] Compan J. et al., "Preferential erosion of carbon composites under intense transient heat pulses", *Physica Scripta*, T128, pp 246-249, 2007

[8] Bonal J. P. and Wu C. H., "Neutron induced thermal properties changes in carbon fiber composites irradiated from 600 to 1000°C", *J. Nucl. Mater.*,230, pp 271-279, 1996

[9] Eto M. et al., "Mechanical properties of neutron-irradiated carbon-carbon composites for plasma facing components", *J. Nucl. Mater.*,212-215, pp 1223-1227, 1994

[10] G. Pintsuk et al., "Mechanical and thermo-physical characterization of the carbon fibre composite NB31", *Physica Scripta*, T128, pp 66-71, 2007

[11] Compan J et al., "Destruction processes of 2- and 3-directional carbon fiber composites under mechanical loads ", Carbon conference 2006 proceedings

[12] Boscary J. et al., "Fabrication and testing of W7-X pre-series target elements", *Physica Scripta*, T128, pp 195-199, 2007

[13] ITER Material Assessment report 2001 G74MA1001-07-11W0.2

[14] Siron O., Pailhes J. and Lamon J., "Modelling of the stress/strain behavior of a carbon/carbon composite with a 2.5 dimensional fibre architecture under tensile and shear loads at room temperature", *Composites Science and Technology*, 59, pp 1-12, 1999

[15] Ogorodnikova O. V., Pestchanyi S., Koza Y., Linke J., "Modelling of thermal shock experiments of carbon based materials in JUDITH", *J. Nucl. Mater.*, 337-339, pp 791-794, 2005